Video Article

Adapting the Electrospinning Process to Provide Three Unique Environments for a Tri-layered *In Vitro* Model of the Airway Wall

Jack C. Bridge[1], Jonathan W. Aylott[2], Christopher E. Brightling[5], Amir M. Ghaemmaghami[3], Alan J. Knox[4], Mark P. Lewis[6], Felicity R.A.J. Rose[1], Gavin E. Morris[1]

[1]Division of Drug Delivery and Tissue Engineering, University of Nottingham

[2]Laboratory of Biophysics and Surface Analysis, School of Pharmacy, University of Nottingham

[3]Division of Immunology and Allergy, School of Molecular Medical Sciences, University of Nottingham

[4]Division of Respiratory Medicine, School of Clinical Sciences, University of Nottingham

[5]NIHR Respiratory Biomedical Research Unit, University of Leicester

[6]School of Sport, Exercise, and Health Sciences, Loughborough University

Correspondence to: Gavin E. Morris at gem8@leicester.ac.uk

URL: http://www.jove.com/video/52986
DOI: doi:10.3791/52986

Keywords: Bioengineering, Issue 101, Electrospinning, 3D Cell Culture, Bioreactor, Airway, Tissue Engineering, *In Vitro* Model

Date Published: 7/31/2015

Citation: Bridge, J.C., Aylott, J.W., Brightling, C.E., Ghaemmaghami, A.M., Knox, A.J., Lewis, M.P., Rose, F.R., Morris, G.E. Adapting the Electrospinning Process to Provide Three Unique Environments for a Tri-layered *In Vitro* Model of the Airway Wall. *J. Vis. Exp.* (101), e52986, doi:10.3791/52986 (2015).

Abstract

Electrospinning is a highly adaptable method producing porous 3D fibrous scaffolds that can be exploited in *in vitro* cell culture. Alterations to intrinsic parameters within the process allow a high degree of control over scaffold characteristics including fiber diameter, alignment and porosity. By developing scaffolds with similar dimensions and topographies to organ- or tissue-specific extracellular matrices (ECM), micro-environments representative to those that cells are exposed to *in situ* can be created.

The airway bronchiole wall, comprised of three main micro-environments, was selected as a model tissue. Using decellularized airway ECM as a guide, we electrospun the non-degradable polymer, polyethylene terephthalate (PET), by three different protocols to produce three individual electrospun scaffolds optimized for epithelial, fibroblast or smooth muscle cell-culture. Using a commercially available bioreactor system, we stably co-cultured the three cell-types to provide an *in vitro* model of the airway wall over an extended time period.

This model highlights the potential for such methods being employed in *in vitro* diagnostic studies investigating important inter-cellular cross-talk mechanisms or assessing novel pharmaceutical targets, by providing a relevant platform to allow the culture of fully differentiated adult cells within 3D, tissue-specific environments.

Video Link

The video component of this article can be found at http://www.jove.com/video/52986/

Introduction

The field of regenerative medicine and tissue engineering is rapidly advancing, with breakthroughs in tracheal and kidney regeneration two notable recent achievements. The biomaterials developed in tissue engineering are becoming more accessible, with opportunities to transfer such protocols to less specialized laboratories. One field primed to benefit through increasing use of biomaterials is *in vitro* diagnostics.

In vitro studies are an important platform to investigate intra-cellular signaling pathways within single cell-types, and have helped delineate mechanisms underlying numerous disease pathophysiologies. These studies generally rely on a single cell-type being cultured as a monolayer on tissue culture plastic (TCP); a two-dimensional (2D) rigid surface far less elastic and porous than the three-dimensional (3D) environment cells are exposed to within a tissue or organ. Animal models have traditionally been employed to confirm effects found *in vitro* also translate to whole tissue, and can also be used as pre-clinical platforms to investigate human diseases. However, inter-species differences undermine this reliance on animal models in our understanding of human disease[-]. For example, much understanding of the lung disease asthma is based upon a mouse model despite inherent differences between the human condition and this model including little evidence of mast cell infiltration of the airway smooth muscle bundle, or the capacity for spontaneous disease development within the animal model[3,4]. There are also ethical considerations regarding the use of animal models, with the “3Rs” standard of “replacement, refinement, and reduction” in animal experimentation being encouraged in the UK and other countries.

An attractive alternative would be the recapitulation of human tissue *in vitro* creating structures to investigate the cooperative nature between adult human cell types in a single unit. Cells exist in 3D multi-cellular structures within tissue, each within a unique micro-environment. The culturing of cells on TCP only allows the culture of cell monolayers, unable to replicate this environment, or provide the capacity for multi-cell

Copyright © 2015 Creative Commons Attribution-NonCommercial-NoDerivs 3.0 Unported License

culture. Biomaterials advancement provides the opportunity to develop both natural and synthetic 3D platforms for cell culture. Decellularized ECM can be used for 3D cell culture when recellularized with other cell-types including stem cells[1], however such protocols can be complex and time consuming, with the availability of tissue limited and largely of non-human origin. Other protocols allow greater control over the cellular environments created such as nanoimprinting, ECM deposition, cell sheet technologies, or electrospinning. Electrospinning creates non-woven 3D porous mats of fibers with diameters ranging from nanometer to micrometer, replicating natural ECM dimensions. Electrospun scaffolds are increasingly being employed as 3D cell culturing platforms[-]. Manipulation of the electrospinning parameters allows intricate control over scaffold characteristics such as pore size, fiber diameter, topography and alignment, and surface chemistry. Alterations of such parameters have been shown to directly affect cell adhesion and growth, when cells were cultured in isolation.

These advantages have been exploited in the present study to allow the culturing of multiple cell types as a single 3D tissue construct, using the airway bronchiole as a model 3D tissue structure. The bronchiole wall consists of three main regions (**Figure 1**). The mucosa is where airway epithelial cells sit at the air-liquid interface (ALI), providing an important barrier to the external environment. They reside on the reticular basement membrane (RBM), a tightly compact ECM comprised mainly of collagen IV, perlecans, and laminins. The sub-mucosal layer is found directly below the mucosa, a more porous region comprised of multiple cell types including fibroblasts, myofibroblasts and infiltrating leukocytes under disease conditions. Finally smooth muscle bundles wrap around the airway in a helical fashion, and are comprised of aligned sheets of airway smooth muscle (ASM). It is the smooth muscle's relative contractile state that controls airway tone. The employment of electrospun scaffolds within the pulmonary system had until recently been limited to regenerative purposes; with an electrospun tracheal replacement being successfully transplanted. Whilst successful, such treatments are limited in numbers, and are focused upon the trachea due to the relative simple nature of the tissue's function. Limited examples of airway models used for *in vitro* diagnostics exist, and are mainly focused on smooth muscle contraction measurements[-]. The non-toxic and non-degradable polymer polyethylene terephthalate (PET) has previously been electrospun, and was employed in the present study to ensure scaffolds produced could be stored for long periods without degrading (allowing them to be used "off the shelf"), and also be suitable for stable cell culture over extended time periods. Previous studies from our group have shown that employing three variations of a basic electrospinning protocol, three individual PET electrospun scaffolds can be produced to provide optimal topographies for culturing airway epithelial, fibroblast, and smooth muscle cells in isolation[21,22] and the coculture of airway epithelial and fibroblast cells[22]. Fiber diameter was found to greatly affect epithelial functionality[22], and fiber alignment allowed the generation of aligned sheets of smooth muscle[21]. These studies were performed independently of each other under static conditions. In the present study, these different scaffolds, containing fully differentiated adult human cells have been cocultured for one week at the ALI in a commercially available bioreactor as a 3D section of the airway wall, providing a physiologically relevant *in vitro* model to investigate airway inter-cellular responses. Whilst this protocol is using the airway bronchiole as a model system, it could be adapted as a platform for the 3D coculture of mucosal units from other organs.

Protocol

Primary ASM cells from non-asthmatic individuals were isolated from bronchial biopsies at the Glenfield Hospital (Leicester, UK) as described previously. The research was approved by the Leicestershire Ethics Committee and patients gave their written, informed consent.

1. Electrospinning PET Scaffolds (Figure 2)

1. Prepare a solution (10 ml) of drink bottle grade PET in a 1:1 dichloromethane (DCMro) – trifluoroacetic acid (TFA) solution. PET concentrations of 8%, 30% and 10% weight/volume *(wt/vol)* are required for nanofiber, microfiber and aligned scaffolds respectively and then stir the solution O/N at RT for the PET to dissolve.
2. Transfer the PET solution into a syringe and attach a 23-G (for nanofiber) or an 18-G (for microfiber and aligned) needle to the syringe and place the syringe into a motorised syringe pump. Make sure the point of the needle is rotated to the bottom.
3. Position the mandrel 15 cm away from the tip of the needle, ensuring the needle is pointed at the centre of the drum.
4. Attach the electricity supply to the needle tip with crocodile clips and ground the mandrel (*via* banana socket) to earth. Switch on the power supply to the mandrel and set speed to 60 rpm (equivalent to approximately 13.2 $m \cdot min^{-1}$) for nanofiber and microfiber scaffolds. Set speed to 2,000 rpm (equivalent to approximately 440 $m \cdot min^{-1}$) for aligned scaffolds.
5. Set the syringe pump to a flow rate of 0.5 $ml \cdot hr^{-1}$ for nanofiber random and aligned scaffolds or 2.0 $ml \cdot hr^{-1}$ for microfiber scaffolds. Allow the pump to run until solution is extruded from the needle tip in order to remove any air in the needle. Then stop the pump.
6. On the syringe pump, set the total volume of solution to be expelled to 2 ml and start the pump.
7. Set voltage supply to 14 kV, and switch on the power supply.
8. Electrospin until 2 ml of solution has been electrospun (4 hr for nanofiber and aligned scaffolds, 1 hr for microfiber scaffolds).
9. Cut the scaffold with a blade along the width of the mandrel. This produces a 2D sheet of scaffold the size of the mandrel surface area (in this case, a rectangular sheet 22 cm x 11 cm) which can be carefully peeled off the mandrel). Store the scaffold in aluminium foil to reduce electrostatic charge).
   Note: Biphasic scaffolds are produced by sequential electrospinning a nanofiber scaffold directly onto a microfiber scaffold.

2. Sterilization of Scaffolds before Use in Cell Culture

1. From the scaffold sheet, punch out discs of biphasic or aligned scaffolds using a 0.8 mm diameter biopsy pen and stick to gasket using non-toxic aquarium glue.
2. Sterilize scaffolds using ultra violet irradiation for 30 min on each side of the scaffolds before soaking in a 20% *vol/vol* antibiotic/ antimycotic solution ($2x10^5$ units ml^{-1} penicillin G, 2,000 mg ml^{-1} streptomycin sulphate and 500 µg ml^{-1} amphotericin B) O/N at 4 °C.
3. Wash scaffolds with PBS 3 times, and then store scaffolds in TCP well plates in PBS at 4 °C until use.

Copyright © 2015 Creative Commons Attribution-NonCommercial-NoDerivs 3.0 Unported License

3. Cell Culture Media Constituents

1. Culture CALU3 epithelial cells in DMEM-F12 media supplemented with 10% *vol/vol* foetal calf serum (FCS), 2 nM L-glutamine solution, 1% *vol/vol* antibiotic/ antimycotic solution (10,000 units ml^{-1} penicillin G, 100 mg ml^{-1} streptomycin sulphate and 25 µg ml^{-1} amphotericin B).
2. Culture MRC5 fibroblast and ASM cells in DMEM media supplemented with 10% *vol/vol* foetal calf serum (FCS), 2 nM L-glutamine solution, 1% *vol/vol* antibiotic/ antimycotic solution (10,000 units ml^{-1} penicillin G, 100 mg ml^{-1} streptomycin sulphate and 25 µg ml^{-1} amphotericin B).
3. Culture epithelial-fibroblast-ASM cell co-cultures in a 70:30 DMEM-F12:DMEM media mixture.

4. Seeding of Fibroblast and Epithelial Cells onto Biphasic Scaffold

1. In a tissue culture plate, soak the scaffolds in DMEM-supplemented media and incubate at 37 °C for 1 hr before cell seeding.
2. Remove the DMEM-supplemented media, place the microfiber phase of scaffold apically and seed 1.5 $x10^4$ MRC5 fibroblast cells in 30 µl of DMEM-supplemented media. Agitate plate on an orbital shaker for 2 hr, before leaving in an incubator at 37 °C 5% CO_2 in air O/N.
3. Turn the scaffold over so the nanofiber phase of scaffold faces apically, seed 3.0 $x10^4$ CALU3 epithelial cells in 30 µl of DMEM–F12-supplemented media onto the nanofiber phase of the scaffold and incubate for 2 hr at 37 °C, 5% CO_2 in air before submerging the scaffold in 70:30 DMEM-F12:DMEM-supplemented media O/N prior to transferring to the bioreactor.

5. Seeding of ASM Cells onto the Aligned Scaffold

1. In a tissue culture plate, soak the scaffolds in DMEM-supplemented media and incubate for 1 hr at 37 °C before seeding 2.5 $x10^4$ cells in 30 µl of DMEM-supplemented media and incubating for 2 hr (37 °C, 5% CO_2 in air). Submerge scaffold in DMEM-supplemented media return to incubator and leave O/N before setting up a tri-culture in the bioreactor.

6. Setting-up the Tri-culture using the Bioreactor System (Figure 7)

1. Place the biphasic scaffold gasket into the groove within one chamber with the epithelial phase facing up into the chamber.
2. Place the aligned scaffold underneath the biphasic scaffold (so it is adjacent to the microfiber phase of the biphasic scaffold) and lock the two chambers of the bioreactor together.
3. Assemble two perfusion flow circuits connected to two medium reservoirs (DMEM-F12-supplemented media in apical reservoir, DMEM-F12/ DMEM-supplemented media in basal reservoir) and pump media around the two circuits at approximately 0.1 ml/min using a peristaltic pump (40 ml media is recycled through each circuit). House all parts of the system within an incubator at 37 °C, 5% CO_2 in air.
4. After one week, remove the media from the apical chamber, and culture the epithelial cells at the ALI for a further week before analysis.

Representative Results

Scanning electron microscope images of decellularized airway tissue or immunohistological images from airway biopsies identified desirable characteristics of the airway ECM we wished to introduce into electrospun scaffold topographies: Native RBM matrix consists of fibers approximately 153 nm ± 30.6 nm (mean ± SD n=50 measurements) in diameter (**Figure 3A & 5A**), whilst the matrix surrounding the RBM was more porous in nature (**Figure 3C**). Immunohistological sections through smooth muscle bundles show ASM present as aligned sheets of cells[21] (**Figure 3E**). This information was used to guide the characteristics introduced into the electrospun scaffolds. A rotating mandrel was able to stably rotate at high speeds (>2,000 rpm/ 440 $m \cdot min^{-1}$) to produce scaffolds with aligned fibers. Slow mandrel rotation (60 rpm 13.2 $m \cdot min^{-1}$) did not affect the fiber orientation, but produced scaffolds with more uniform thickness than when electrospinning onto a static plate. By altering the electrospinning parameters (PET concentration and solution flow rate), it was possible to create scaffolds fibers with diameters of several micrometers or hundreds of nanometers (electrospinning parameters are stated in Table 1).

Electrospun fibers with equivalent fiber diameters to natural RBM fibers (150 nm) were produced using a 6% PET solution, however at such low PET concentrations, beading of the fibers occurred (**Figure 4A**). This was eliminated by increasing the concentration of the PET solution to 8% which produced uniform nanofibers possessing an average diameter of 255 nm ± 2.4 nm (mean ± SEM) and average pore size of 1.43 µm ± 0.02 µm (**Figures 4B, 5A&B**). To electrospin nanofibers it was necessary to reduce the needle size from 18 G to 23 G, allowing slower flow rates whilst maintaining a higher flow velocity and reducing needle blockage, a recurring problem with the larger needle. When electrospinning microfibers, an increase in PET solution to >30 % PET lead to a lack of uniformity in fiber diameter (**Figure 4F**) in addition to multiple blockages at the needle tip due to the high solution viscosity. Uniform microfiber mats possessing an average fiber diameter of 2.50 µm ± 0.02 µm (mean ± SEM) and average pore size of 10.45 µm ± 0.13 µm were produced when electrospinning a 30% *wt/vol* PET solution at a flow rate of 2 mL/ h^{-1} (**Figures 4F, 5A&B**). Sequential electrospinning of the nanofiber scaffold directly onto a microfiber scaffold (still attached to the mandrel) created a biphasic scaffold (**Figure 3D**). The average fiber diameters were 280 nm ± 20 nm and 2.30 µm ± 0.06 µm for the nanofiber and microfiber phases respectively, comparable to dimensions of individual nanofiber and microfiber scaffolds. Additionally, the thickness of the biphasic scaffold was similar to the sum of the individual nanofiber and microfiber scaffolds (**Figure 5C**). Through increasing the mandrel speed (2,000 rpm/440 $m \cdot min^{-1}$), highly aligned nano- or microfiber scaffolds were produced. The 8% *wt/vol* PET solution was not optimal for producing aligned nanofibers and produced fibers possessing a wave-like morphology (**Figure 3F**). An increase to 10% PET nullified this effect, but still resulted in a reduced fiber diameter (216 nm ± 2.2 nm (mean ± SEM)) compared to the randomly aligned nanofiber scaffolds. Fiber alignment was calculated by determining the deviation of each fiber's angle from the mean fiber angle. In aligned nanofiber scaffolds 79% of fibers were aligned (± 10° mean fiber angle) compared to 10.2% of fibers in randomly aligned nanofiber scaffolds (**Figure 5D**).

The 8% nanofiber scaffold was used to recapitulate the RBM on which epithelial cells reside, and was used to support the culture of CALU3 cells (an airway epithelial cell-line). The 30% *wt/vol* microfiber scaffold, being more porous in nature was used to mimic the sub-mucosal region, and was cultured with MRC5 cells (an airway fibroblast cell-line). The 10% *wt/vol* aligned nanofiber scaffold provided topological referencing to ensure ASM cell alignment when cultured on the scaffold. All three cell-types showed an increase in viability when cultured on their individual

Copyright © 2015 Creative Commons Attribution-NonCommercial-NoDerivs 3.0 Unported License

scaffolds over a 2 week period (**Figure 6A**), and expressed cell-type specific proteins after the 2 week culture period (**Figure 6B, 6C, & 6D**). Further characterization of individual cell-scaffold interactions have been reported elsewhere[21]. The sequential electrospinning of the nanofiber scaffold onto the microfiber scaffold produced a biphasic scaffold for the coculture of the CALU3 epithelial cells and MRC5 fibroblast cells onto the nanofiber and microfiber phases respectively. The culturing of the two cells together under static conditions has been reported elsewhere[22]. Further work attempting to add other cell layers or extend biphasic culturing times beyond 2 weeks under static conditions proved unsuccessful (data not shown). To culture a tri-layered model over an extended period, we used a perfusion flow bioreactor. The CALU3 and MRC5 cells were seeded onto the biphasic scaffold, and ASM cells seeded onto an aligned scaffold, and both were cultured separately for 2 days. The two scaffolds were then bought together to form a tri-layer model of the airway wall within the bioreactor (**Figure 7**). Both chambers were perfused with media for 7 days before the apical epithelial chamber had its media removed, and the epithelial cells were cultured at the ALI for a further 7 days. Scaffolds were fixed and either sectioned and stained, or whole scaffolds were immunostained for cell-specific markers. Sections through the tri-layer culture showed cell nuclei distributed through all three layers of the coculture (**Figure 8B**). When cells were immunostained for cell-specific markers, epithelial cells populated the apical nanofiber phase as a confluent cell-layer and stained positive for cytokeratin (**Figure 8C**), on the microfiber phase, fibroblasts stained positive for S100A4 (**Figure 8D**), and on the aligned 10% scaffold ASM cells stained positive for SM22α (**Figure 8E**), indicating good survival of each cell-type within the 3D model of the airway wall.

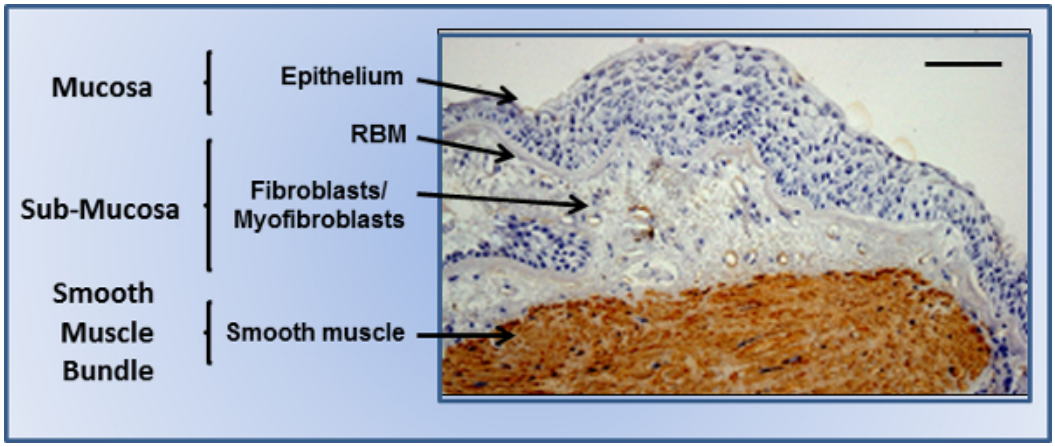

Figure 1. The airway bronchiole. Bronchial biopsy from a severe asthmatic airway showing the epithelium on the reticular basement membrane (RBM), with the underlying submucosal region populated with mesenchymal cells, and the surrounding smooth muscle bundles populated with smooth muscle cells stained for smooth muscle alpha-actin (brown). Scale bar indicates 200 μm. Please click here to view a larger version of this figure.

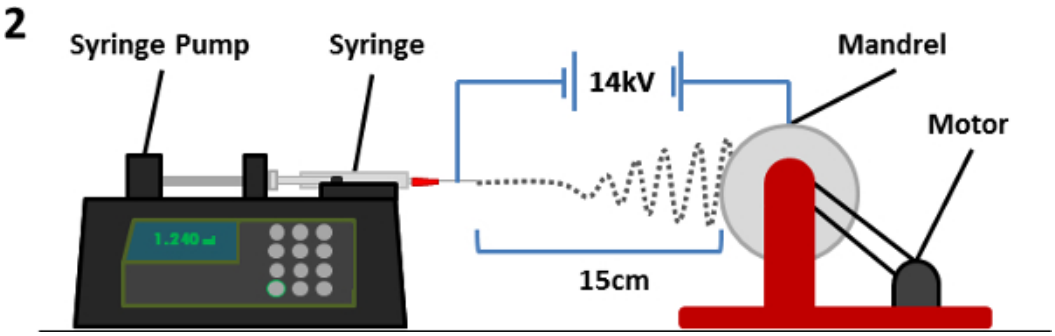

Figure 2. A schematic of the electrospinning equipment. A syringe containing the polymer/solvent solution (with needle attached) is placed on a syringe pump facing the mandrel. An electric potential is established between the needle and mandrel causing fibers to be ejected from the needle tip and deposited on the rotating mandrel. As the fiber passes through the atmosphere, the solvent evaporates causing deposition of polymer fibers on the mandrel. Please click here to view a larger version of this figure.

Copyright © 2015 Creative Commons Attribution-NonCommercial-NoDerivs 3.0 Unported License

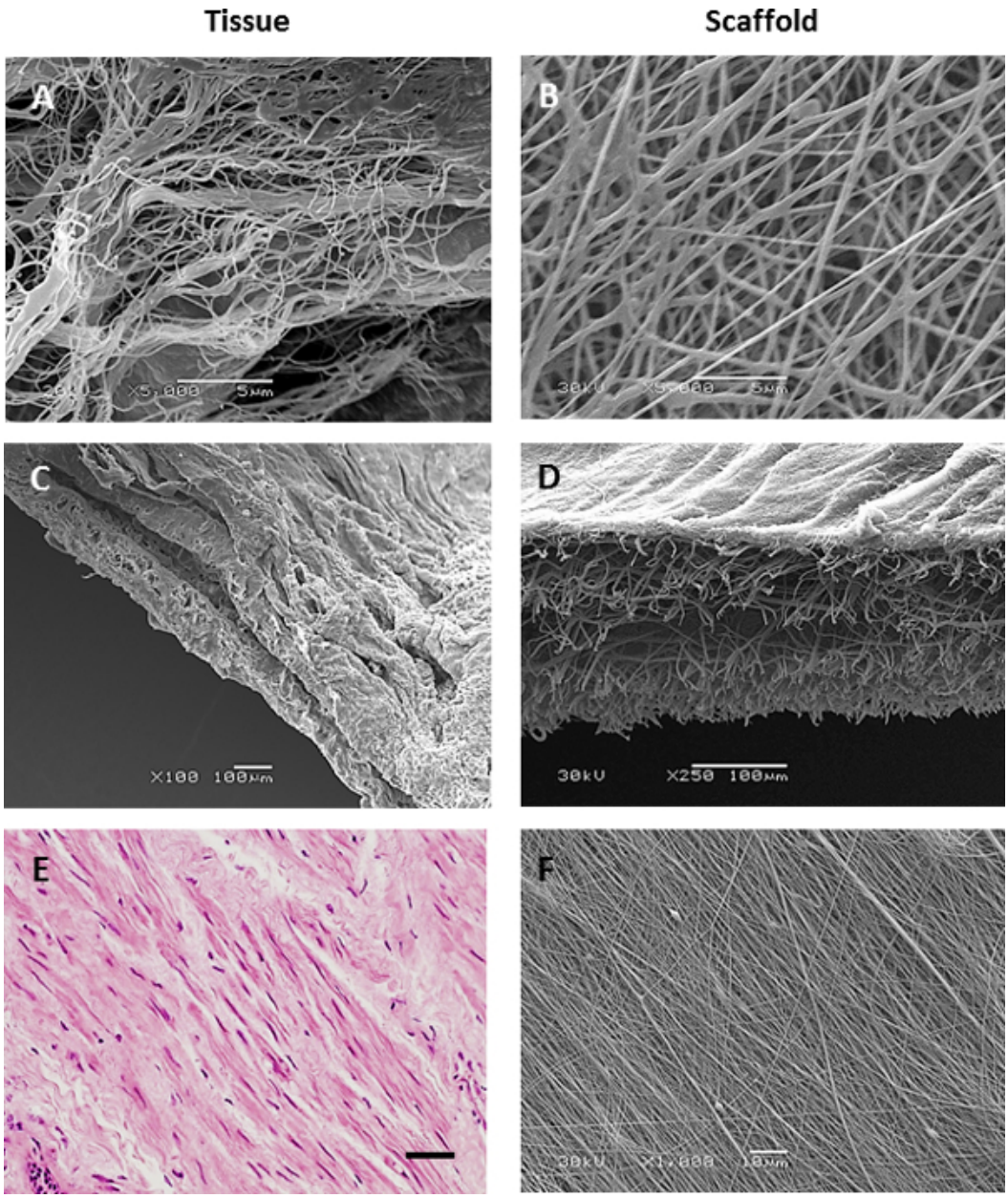

Figure 3. Comparison of electrospun scaffolds to native airway ECM. Scanning electron microscope images of decellularized basement membrane (**A**), decellularized airway bronchiole cross section (**C**) and a histological section of an airway smooth muscle bundle (stained with haematoxylin and eosin, scale bar 40 μm) (**E**) compared with nanofiber (**B**) biphasic (**D**) and aligned (**F**) PET scaffolds. Please click here to view a larger version of this figure.

Table 1. Parameters used for electrospinning the microfiber, nanofiber and aligned scaffolds individually and for the biphasic scaffold.

Copyright © 2015 Creative Commons Attribution-NonCommercial-NoDerivs 3.0 Unported License

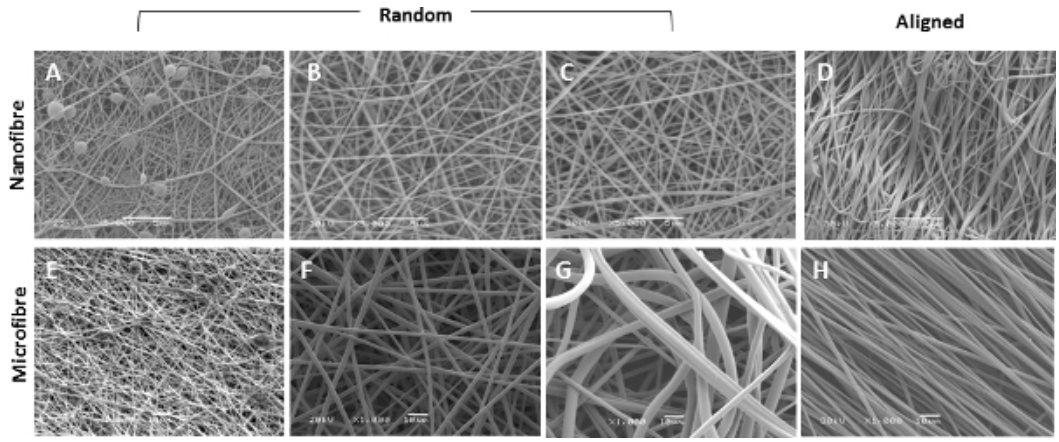

Figure 4. Alteration in PET concentrations affects fiber characteristics. Scanning electron microscope images of electrospun scaffolds spun from 6%, 8%, 10% (**A-C**), 25%, 30% and 35% (**E-G**) (*wt/vol*) PET solutions. Also shown are aligned scaffolds produced from 8% (**D**) and 30% (**H**) *wt/vol* PET solutions. **A-D** imaged at 5,000X magnification, **E-H** imaged at 1,000X magnification. Please click here to view a larger version of this figure.

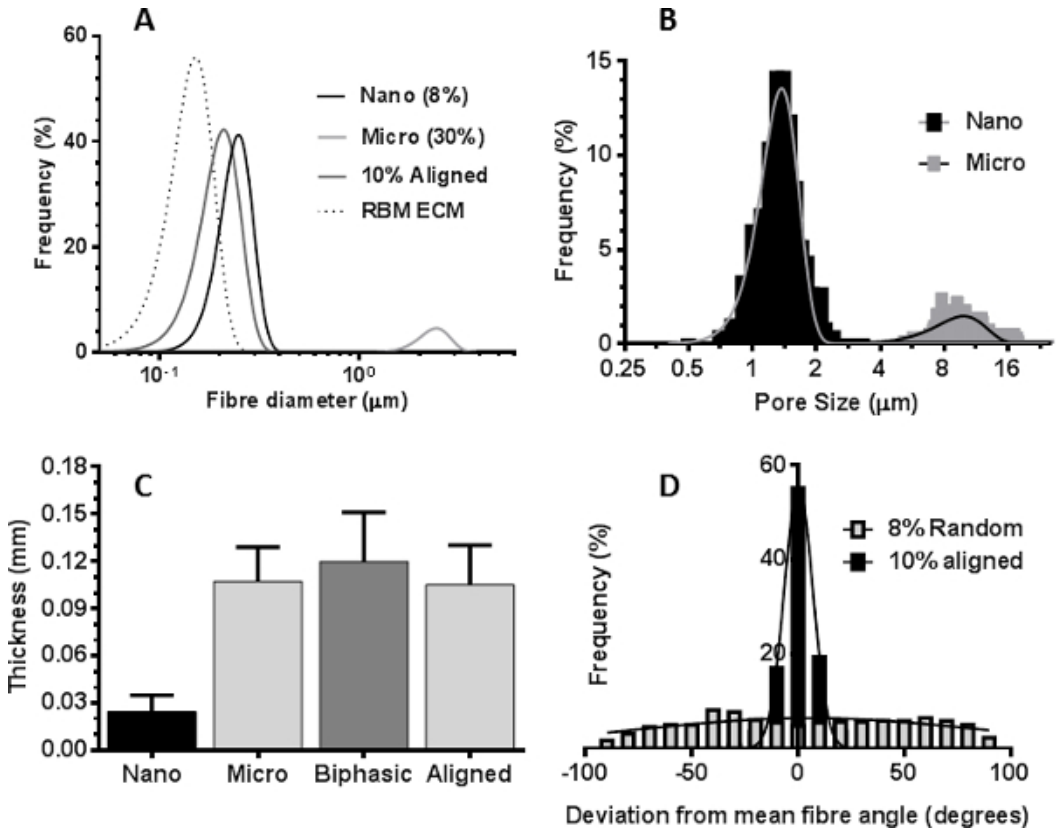

Figure 5. Properties of electrospun PET scaffolds. (**A**) Distribution curves showing fiber diameter distribution from the reticular basement membrane extracellular matrix (RBM ECM), randomly aligned nano- and micro-fiber scaffolds, and the aligned nanofiber scaffold. (**B**) Histogram showing the relative pore size distribution in nano- and micro-fiber scaffolds. (**C**) Average thickness of the nanofiber, microfiber, biphasic and aligned scaffolds (mean±standard deviation, n=6). (**D**) Histogram plot showing the deviation from mean fiber orientation in random or aligned nanofiber scaffolds Scaffold fiber analysis was carried out using ImageJ software. Please click here to view a larger version of this figure.

Copyright © 2015 Creative Commons Attribution-NonCommercial-NoDerivs 3.0 Unported License

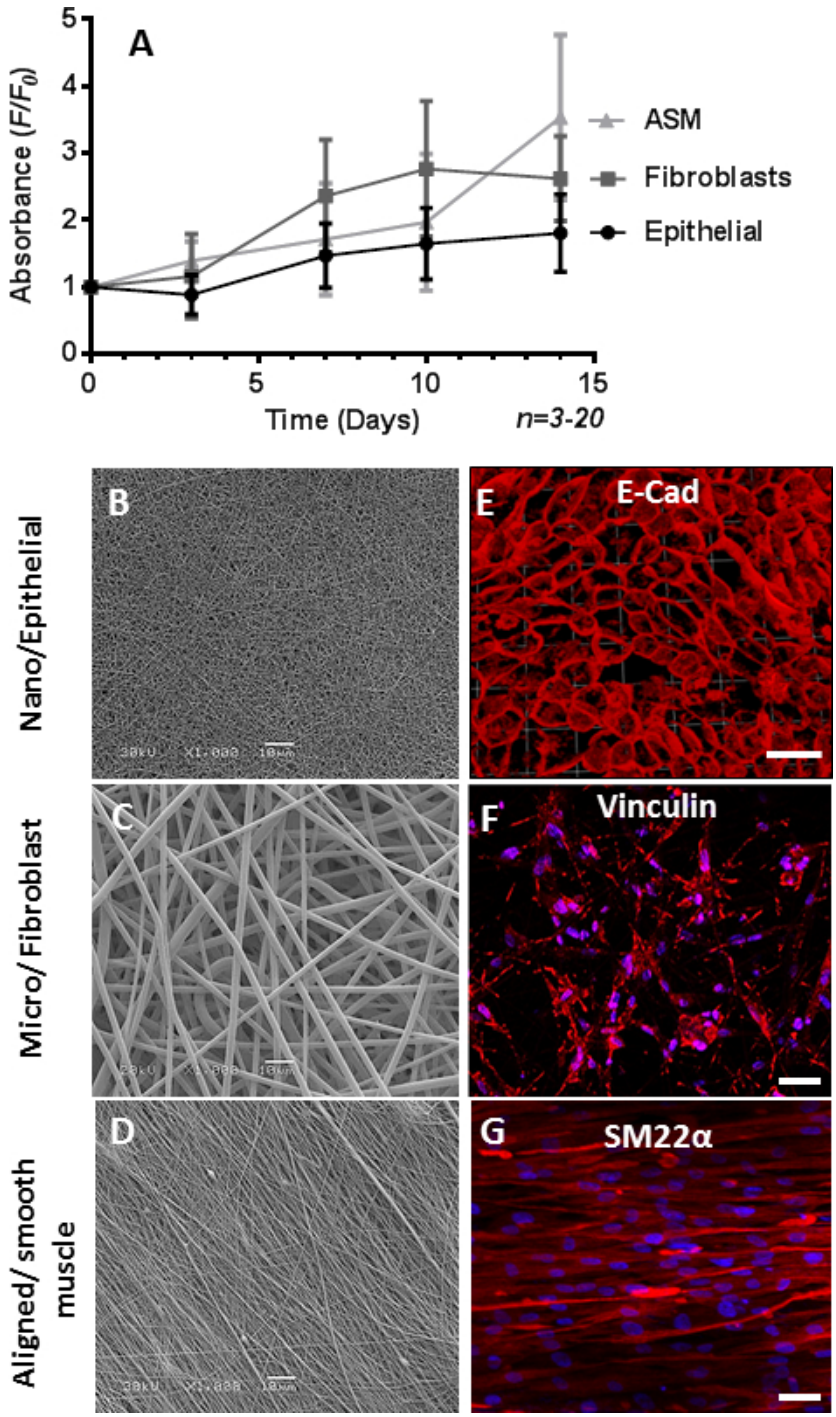

Figure 6. The culture of the individual cell types on the individual scaffolds. (**A**) alamarBlue cell viability assay results for ASM cells on aligned scaffolds, CALU3 cells on nanofiber scaffolds and MRC5 cells on microfiber scaffolds (mean±SEM, n=3-20). Scanning electron microscope images of the nanofiber, microfiber and aligned fiber scaffolds (**B**,**C** and **D** respectively) and immunofluorescent images of CALU3 cells stained for E-cadherin (red), MRC5 cells stained for vinculin (red) and ASM cells stained for SM22α (red) all on their specialised scaffold (**E**, **F** and **G** respectively). Hoechst was used to stain nuclei (blue), scale bar indicates 40 μm. Please click here to view a larger version of this figure.

Copyright © 2015 Creative Commons Attribution-NonCommercial-NoDerivs 3.0 Unported License

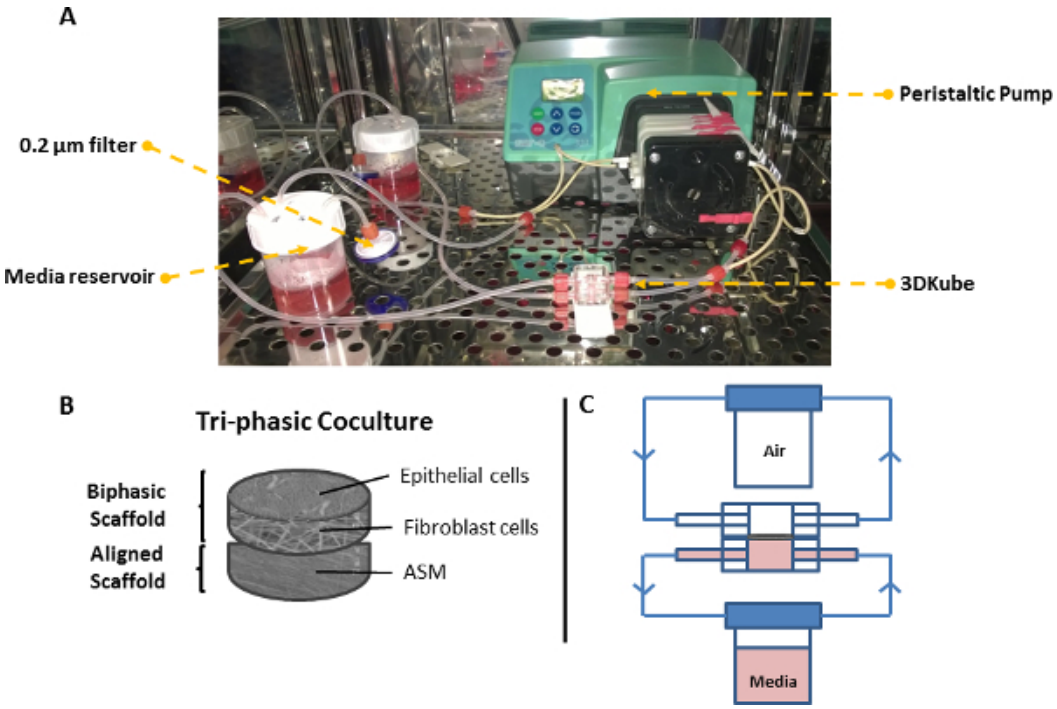

Figure 7. Perfusion system for tri-layer airway wall model. (**A**) Photograph of bioreactor vessel connected to peristaltic pump and 2x media reservoirs. (**B**) Schematic of the tri-layered scaffolds. (**C**) Schematic of the two bioreactor circuits when the airway model is held at the air-liquid interface. Please click here to view a larger version of this figure.

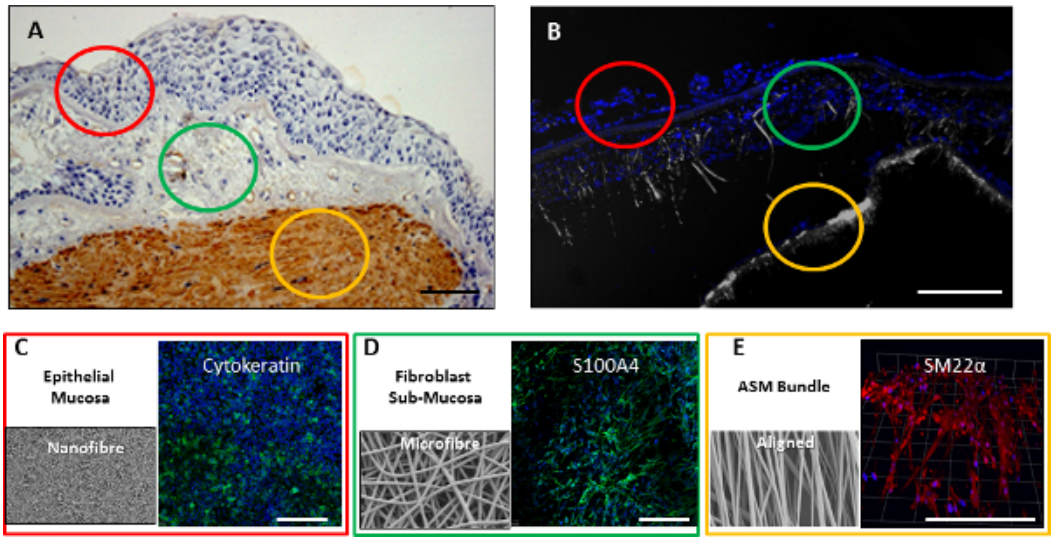

Figure 8. Complete 3D airway wall model. (**A**) Bronchial biopsy of airway wall with the mucosal layer highlighted in red, the submucosal region highlighted in green, and the smooth muscle bundle highlighted in gold. (**B**) Section through tri-layered airway wall consisting of biphasic and aligned scaffolds populated with epithelial, fibroblast and smooth muscle cells fixed after 2 weeks coculture. Cell nuclei were stained with DAPI (blue) with scaffold reflectance (grey) concurrently imaged. Scaffolds were also fixed and immunostained for cell specific markers after 2 weeks, with CALU3 cells stained for cytokeratin (green) (**C**), MRC5 cells stained for S100A4 (green) (**D**), and smooth muscle cells stained for SM22α (red) (**E**). Scale bar indicates 200 µm. Please click here to view a larger version of this figure.

Copyright © 2015 Creative Commons Attribution-NonCommercial-NoDerivs 3.0 Unported License

	Scaffold	Polymer conc. (*wt/vol*)	Solvent Mix (DCM:TFA)	Flow Rate (ml h^{-1})	Needle Gauge (G)	Volume (ml)	Distance (cm)	Mandrel speed (rpm)
Individual	Microfibre	8%	1:1	0.5	23	2.0	15	60
	Nanofibre	30%	1:1	2.0	18	2.0	15	60
	Aligned fibre	10%	1:1	0.5	18	2.0	15	2000
Biphasic	1. Microfibre	30%	1:1	2.0	18	2.0	15	60
	2. Nanofibre	8%	1:1	0.5	23	1.5	15	60

Table 1.

Discussion

The ability to electrospin polymeric fibers with structural properties comparable to natural ECM has led to numerous natural or synthetic polymers, or polymer blends being electrospun to recreate these environments[1]. Manipulation of the process parameters (including polymer choice, polymer concentration, solvent, needle tip distance and temperature) can all influence scaffold characteristics; however some parameters can have greater impact on scaffold properties than others[25]. When modifying PET fiber diameter, we found the key parameters to be the concentration of the polymer used, the rate at which the polymer solution was electrospun, and the needle's diameter. When electrospinning aligned fibers the key parameters are the collection method used (a rotating mandrel), and the speed at which the mandrel rotates. Through reducing the mandrel speed to 60 rpm, we found the randomly aligned scaffolds produced showed greater scaffold uniformity compared to electrospinning onto a flat collector plate.

The characteristics of decellularized airway tissue were analysed to provide guidance for the various scaffold topographies developed for the culture of each airway cell-type. Electrospun nanofibers are an attractive scaffold to replicate basement membrane structures due to the small pore size but high overall porosity that allows for increased metabolite diffusion whilst restricting cellular movement.[9] Whilst optimising the electrospinning parameters, a range of PET concentrations and flow rates were tested. The thinnest fibers were achieved using a 6% *wt/vol* PET solution, previously used by other groups. However, high levels of beading, and a lack of uniformity were constant problems. Initial attempts to remove the beading included adding a cationic surfactant, cetyltrimethylammonium bromide (CTAB), to the solution to lower the surface tension, and testing various sources of PET. The addition of surfactant reduced the amount of beading, but not fully. After trying a number of commercial sources of PET pellets, food grade drink bottle PET was used, by cutting up drinks bottles and dissolving these in the DCM:TFA solvent solution. Using this as the PET source resulted in an increase in fiber uniformity and a reduction in fiber beading. By increasing the solution concentration slightly to 8% *wt/vol* and reducing the needle diameter (18G to 23G) we consistently produced defect free nanofibers with a fiber diameter of approximately 250 nm. Electrospun nanofiber scaffolds can be highly electrostatic upon collection from the mandrel making manual handling of the scaffolds difficult. This was improved by storing the scaffolds in aluminium foil after spinning and soaking in 70% IMS before use. This appeared to help dissipate the residual electrostatic charge left on the scaffold from the electrospinning process.

To provide topographies similar to the individual microenvironments encountered by the three main airway cell types within the airway wall, a basic electrospinning protocol was adapted to produce three unique scaffolds for these cell types: by electrospinning a low concentration PET solution slowly, randomly aligned nanofibers were generated, *onto* which epithelial cells were seeded (mimicking the RBM). By electrospinning a higher concentration PET solution at a faster rate, randomly aligned microfibers were generated (producing a more porous scaffold), *into* which fibroblasts were seeded (mimicking the sub-mucosal area immediately beneath the RBM). By electrospinning a low concentration PET solution onto a high velocity rotating mandrel aligned nanofibers were produced, onto which smooth muscle cells orientated in the fiber direction, producing aligned sheets of cells.

Increased fiber diameters lead to increased pore size, allowing greater cell penetration into scaffolds and so help create a true 3D environment[1]. Microfiber scaffolds were employed for the culture of fibroblasts in the study to ensure that the cells resided on multiple planes within the scaffold. By increasing the PET concentration to 30% *wt/vol*, PET fibers with an average diameter of 2.5 µm were produced. Greater diameter fibers (≈ 4 µm) were produced using a 35% *wt/vol* PET solution, but scaffold thickness uniformity was lost, and higher variability between individual fibers was apparent. Pores in the microfiber scaffold were over 7 times greater than those measured in the nanofiber scaffolds (10.45 µm vs 1.43 µm respectively), but still static seeding of cells provided limited cellular penetration. This was improved by dynamically seeding the cells using an orbital mixer, a method shown to be effective previously.

Highly aligned nanofiber scaffolds were created by electrospinning a 10% *wt/vol* PET solution onto the mandrel rotating at 2,000 rpm (≈ 440 $m \cdot min^{-1}$). The PET concentration was increased from 8% to prevent an irregular wave-like morphology that fibers exhibited at lower concentrations. Despite the increase in concentration, aligning the fibers reduced the average fiber diameter (216 nm vs. 255 nm, aligned vs. random). The high speed of the mandrel drawing the fibers out before they have dried is likely to cause this effect. The alignment of the fibers influenced the alignment of ASM cells, and also has other physiological effects on the ASM cells which have been characterized elsewhere[21].

The major limitation of this protocol is the inability to image live cells on/in the scaffolds making initial cell-attachment or differentiation over an extended time period impossible to determine without sacrificing samples. This means most optimization occurs after the culture period; *i.e.,* fixing samples and then measuring whether cell culture was successful *after* not *during* cell culture. Observing a color change in scaffolds incubated in alamarBlue (blue to pink) indicates cells are present and viable, but is not ideal. Electrospinning more transparent polymers such as gelatin could aid in visualizing cells on the scaffolds. The electrospinning of a nanofibrous scaffold within our model allowed the replication of

Copyright © 2015 Creative Commons Attribution-NonCommercial-NoDerivs 3.0 Unported License

the airway RBM, similarly comprised of dense nanofibers on which the epithelial cells reside. It has previously been shown that structural cells cannot migrate through the nanofiber scaffold[22], although immune cells are able to (data not shown). Whilst advantageous for the culturing of specific cell-types on a 3D surface (such as epithelial and endothelial cells), this prevention of structural cell migration through the nanofibers may be detrimental for the culturing of other cell types. As smooth muscle is unable to migrate through the aligned nanofiber scaffold we assembled the tri-layered coculture with the smooth muscle and fibroblast layers facing each other (opposed to the aligned scaffold separating the two cell types). Whilst this allows the cells to be in close apposition, the current study cannot conclude whether one cell type (either the fibroblast or smooth muscle) would overtake the whole layer over a more prolonged culture period. Despite these limitations, a viable tri-layer model of the airway wall has been developed that provides an alternative platform to investigate the interactions between these multiple cell-types. A similar tri-layered study has recently been published where fibroblasts were embedded within a cylindrical collagen I hydrogel with smooth muscle seeded on the outer surface and epithelial cells within the luminal surface[17]. The mechanical stability of the electrospun scaffolds developed here would allow similar tubular constructs to be formed, and remains a current research aim within our group. Whilst the study has focused on the airway, several organs within the body share this basic mucosal structural unit, and through modifying the tenants highlighted in this study, similar platforms could be developed for tissues containing a basement membrane unit including blood vessels, the bladder and the cornea, where collagen based multi-layered models have been employed.

Disclosures

The Authors have nothing to disclose.

Acknowledgements

The research leading to these AirPROM results has received funding from the European Union under grant agreement n° 270194.This work was also funded by the National Centre for the Replacement, Refinement, and Reduction of Animals in Research (NC3Rs), and the Engineering and Physical Research Centre (EPSRC) Doctoral Training Centre (DTC) in Regenerative Medicine, U.K.

References

1. Macchiarini, P., *et al.* Clinical transplantation of a tissue-engineered airway. *Lancet.* **372**, (9655), 2023-2030 (2008).
2. Song, J., Guyette, J., Gilpin, S. Regeneration and experimental orthotopic transplantation of a bioengineered kidney. *Nature medicine.* **19**, (5), 646-651 (2013).
3. Wenzel, S., Holgate, S. The mouse trap: it still yields few answers in asthma. *American journal of respiratory and critical.* **174**, (11), 1171-1173 (2006).
4. Zosky, G. R., Sly, P. D. Animal models of asthma. *Clinical and experimental allergy journal of the British Society for Allergy and Clinical Immunology.* **37**, (7), 973-988 (2007).
5. Bates, J. H. T., Rincon, M., Irvin, C. G. Animal models of asthma. American journal of physiology. *Lung cellular and molecular physiology.* **297**, (3), L401-L410 (2009).
6. Johansson, F., Carlberg, P., Danielsen, N., Montelius, L., Kanje, M. Axonal outgrowth on nano-imprinted patterns. *Biomaterials.* **27**, (8), 1251-1258 (2006).
7. Paik, I., *et al.* Rapid micropatterning of cell lines and human pluripotent stem cells on elastomeric membranes. *Biotechnology and bioengineering.* **109**, (10), 2630-2641 (2012).
8. Williams, C., *et al.* Aligned Cell Sheets Grown on Thermo-Responsive Substrates with Microcontact Printed Protein Patterns. *Advanced Materials.* **21**, (21), 2161-2164 (2009).
9. Schindler, M., *et al.* A synthetic nanofibrillar matrix promotes in vivo-like organization and morphogenesis for cells in culture. *Biomaterials.* **26**, (28), 5624-5631 (2005).
10. Schindler, M., *et al.* Living in Three Dimensions. *Cell Biochemistry and Biophysics.* **45**, (14), 215-227 (2006).
11. Ahmed, I., *et al.* Morphology, cytoskeletal organization, and myosin dynamics of mouse embryonic fibroblasts cultured on nanofibrillar surfaces. *Molecular and Cellular Biochemistry.* **301**, (1-2), 241-249 (2007).
12. Flemming, R., Murphy, C., Abrams, G. Effects of synthetic micro-and nano-structured surfaces on cell behavior. *Biomaterials.* **20**, 573-588 (1999).
13. Sun, T., *et al.* Development of a 3D Cell Culture System for Investigating Cell Interactions With Electrospun Fibers. *Biotechnol. Bioeng.* **97**, (5), 1318-1328 (2007).
14. Kim, D. -H., Provenzano, P. P., Smith, C. L., Levchenko, A. Matrix nanotopography as a regulator of cell function. *The Journal of cell biology.* **197**, (3), 351-360 (2012).
15. Jeffery, P. K. Remodeling in Asthma and Chronic Obstructive Lung Disease. *American Journal of Respiratory and Critical Care Medicine.* **164**, (10 pt 2), S28-S38 (2001).
16. Jungebluth, P., *et al.* Tracheobronchial transplantation with a stem-cell-seeded bioartificial nanocomposite: a proof-of-concept study. *Lancet.* **378**, (9808), 1997-2004 (2011).
17. Miller, C., George, S., Niklason, L. Developing a tissue-engineered model of the human bronchiole. *Journal of Tissue Engineering and Regenerative.* (July), 619-627 (2010).
18. West, A. R., *et al.* Development and characterization of a 3D multicell microtissue culture model of airway smooth muscle. American journal of physiology. *Lung cellular and molecular physiology.* **304**, (1), L4-L16 (2013).
19. Nesmith, A. P., Agarwal, A., McCain, M. L., Parker, K. K. Human airway musculature on a chip: an in vitro model of allergic asthmatic bronchoconstriction and bronchodilation. *Lab on a chip.* (2014).
20. Hadjizadeh, A., Ajji, A., Bureau, M. N. Nano/micro electro-spun polyethylene terephthalate fibrous mat preparation and characterization. *Journal of the mechanical behavior of biomedical materials.* **4**, (3), 340-351 (2011).
21. Morris, G., *et al.* Human airway smooth muscle maintain in situ cell orientation and phenotype when cultured on aligned electrospun scaffolds. *American Journal of Physiology - Lung Cellular and Molecular Physiology.* **307**, (1), L38-L47 (1999).

Copyright © 2015 Creative Commons Attribution-NonCommercial-NoDerivs 3.0 Unported License

22. Morris, G. E., *et al.* A novel electrospun biphasic scaffold provides optimal three-dimensional topography for in vitro co-culture of airway epithelial and fibroblast cells. *Biofabrication.* **6**, (3), 035014 (2014).
23. Sell, S., *et al.* The Use of Natural Polymers in Tissue Engineering: A Focus on Electrospun Extracellular Matrix Analogues. *Polymers.* **2**, (4), 522-553 (2010).
24. Subbiah, T., Bhat, G. S., Tock, R. W., Parameswaran, S., Ramkumar, S. S. Electrospinning of nanofibers. *Journal of Applied Polymer Science.* **96**, (2), 557-569 (2005).
25. Dalton, P. D., *et al.* Electrospinning and additive manufacturing: converging technologies. *Biomaterials Science.* **1**, (2), 171 (2013).
26. Boland, E. D., Wnek, G. E., Simpson, D. G., Pawlowski, K. J., Bowlin, G. L. Tailoring tissue engineering scaffolds using electrostatic processing techniques: A study of poly(glycolic acid) electrospinning. *Journal of Macromolecular Science-Pure and Applied Chemistry.* **38**, (12), 1231-1243 (2001).
27. Stitzel, J. D., Bowlin, G. L., Mansfield, K., Wnek, G. E., Simpson, D. G. Electrospraying and electrospinning of polymers for biomedical applications. Poly(lactic-co-glycolic acid) and poly(ethylene-co-vinylacetate). *Revolutionary Materials: Technology And Economics.* **32**, 205-211 (2000).
28. Liu, W., Thomopoulos, S., Xia, Y. Electrospun nanofibers for regenerative medicine. *Advanced healthcare materials.* **1**, (1), 10-25 (2012).
29. Veleirinho, B. Solvent and concentration effects on the properties of electrospun poly (ethylene terephthalate) nanofiber mats. *Journal of Polymer.* 460 (2008).
30. Balguid, A., *et al.* Tailoring Fiber Diameter in Electrospun Poly(epsilon-Caprolactone) Scaffolds for Optimal Cellular Infiltration in Cardiovascular Tissue Engineering. *Tissue Engineering Part A.* **15**, (2), 437-444 (2009).
31. Shalumon, K. T., *et al.* Fabrication of three-dimensional nano, micro and micro/nano scaffolds of porous poly(lactic acid) by electrospinning and comparison of cell infiltration by Z-stacking/three-dimensional projection technique. *IET nanobiotechnology / IET.* **6**, (1), 16-25 (2012).
32. Thevenot, P., Nair, A., Dey, J., Yang, J., Tang, L. Method to Analyze Three-Dimensional Cell Distribution and Infiltration in Degradable Scaffolds. *Tissue Engineering Part C-Methods.* **14**, (4), 319-331 (2008).
33. Rose, J., *et al.* Gelatin-Based Materials in Ocular Tissue Engineering. *Materials.* **7**, (4), 3106-3135 (2014).
34. Liliensiek, S. J., Nealey, P., Murphy, C. J. Characterization of Endothelial Basement Membrane Nanotopography in Rhesus Macaque as a Guide for Vessel Tissue Engineering. *Tissue Engineering Part A.* **15**, (9), (2009).
35. Abrams, G. A., Murphy, C. J., Wang, Z. -Y., Nealey, P. F., Bjorling, D. E. Ultrastructural basement membrane topography of the bladder epithelium. *Urological research.* **31**, (5), 341-346 (2003).
36. Abrams, G. A., Bentley, E., Nealey, P. F., Murphy, C. J. Electron Microscopy of the Canine Corneal Basement Membranes. *Cells Tissues Organs.* **170**, (4), 251-257 (2002).
37. Reichl, S., Bednarz, J., Muller-Goymann, C. Human corneal equivalent as cell culture model for in vitro drug permeation studies. *British Journal of Ophthalmology.* **88**, (4), 560-565 (2004).

Copyright © 2015 Creative Commons Attribution-NonCommercial-NoDerivs 3.0 Unported License